

Variations of the Hawaiian hot spot activity revealed by variations in the magma production rate

V. Vidal and A. Bonneville

Laboratoire de Géosciences Marines, Institut de Physique du Globe, Centre National de Recherche Scientifique, Paris, France

Received 28 April 2003; revised 10 December 2003; accepted 26 December 2003; published 16 March 2004.

[1] In order to evaluate the activity of the Hawaiian hot spot, we calculate both the magma production rate, associated with volcanism, and the rate of swell formation, characteristic of the plume behavior. Both computations are made along the Emperor-Hawaii track. Depth anomaly is calculated by correcting the 2' bathymetry grid of *Smith and Sandwell* [1997] from thermal subsidence. A new filtering method is then used to separate the topography associated with volcanism and the swell surrounding the hot spot chain. The volume of magma includes the compensating root underlying the volcanoes, computed assuming either an Airy compensation (local) or a flexural root (regional) associated with the volcanic load. Next, the volume corresponding to the swell is calculated between the swell amplitude map and the zero value of the depth anomaly. Temporal variations of both volumes are then computed by the means of $1^\circ \times 10^\circ$ windows translated along the hot spot track. Both volume fluxes are correlated through time and present (1) a general increase in amplitude for the last 30 Ma, indicating an increase in hot spot activity, and (2) short-wavelength oscillations with a 5 m.y. period, which may reflect the presence of solitary waves in the plume conduit. Contrary to the swell volume flux, the magma production rate estimation is not dependent on the subsidence model and is still valid for the older part of the chain. It is thus the most relevant parameter to describe the temporal variation of the Hawaiian hot spot behavior. **INDEX TERMS:** 8120 Tectonophysics: Dynamics of lithosphere and mantle—general; 8121 Tectonophysics: Dynamics, convection currents and mantle plumes; 8145 Tectonophysics: Physics of magma and magma bodies; 9355 Information Related to Geographic Region: Pacific Ocean; **KEYWORDS:** Hawaii, hot spot, temporal variations, mantle plume

Citation: Vidal, V., and A. Bonneville (2004), Variations of the Hawaiian hot spot activity revealed by variations in the magma production rate, *J. Geophys. Res.*, 109, B03104, doi:10.1029/2003JB002559.

1. Introduction

[2] The concept of hot spots and mantle plumes first appeared to explain the formation of linear seamount chains such as the Hawaiian Islands [*Wilson*, 1963]. Since the hot spot activity may last for many millions years (at least 70 Ma for Hawaii), an interesting point to study is their variability through time. Two main surface manifestations generally associated with a hot spot can give a good basis to the determination of its strength and temporal variations. The first parameter is the production rate of volcanic material Q_v . It corresponds to the total volume of material brought by the hot spot in a given time, including the volume of the volcanic edifices, and the compensating root, right under the edifice, due to flexural deformation of the plate, with an eventual underplating component. The second parameter is the volume flux Q_s , associated with the positive depth anomaly surrounding hot spots, called a swell [*Crough*, 1983; *McNutt*, 1998]. The swell is a direct consequence of the buoyant mantle upwelling. Assuming

depth compensation, the rate of swell formation, or buoyancy flux, is given by

$$B = (\rho_m - \rho_w)AV_p = \overline{\Delta\rho_p}Q_p, \quad (1)$$

where ρ_m and ρ_w are mantle and seawater densities respectively, A is the area of the swell in a vertical plane transverse to the hot spot track, V_p plate velocity in the hot spot frame, Q_p denotes the plume volume flux and $\overline{\Delta\rho_p}$ the average density reduction in the volume flux per time for the plume [*Sleep*, 1990].

[3] The buoyancy parameter B seems the most appropriate to quantify the hot spot activity. However, its use becomes irrelevant over long periods of time, due to the own subsidence of the hot spot swell. It is more relevant to determine the production rate of volcanic material Q_v , but this latter parameter only characterizes the surface manifestation of a hot spot, and not the plume flux. The degree of melting can link both parameters, but needs to be known, which is not the case all along the Emperor-Hawaii chain. However, *Phipps Morgan et al.* [1995] deduce from both the volume of hot spot volcanism and the size of the swell that they have a shared origin. That is why we propose here

a comparison of the variations of the two parameters Q_v and Q_s (or B) all along the hot spot chain. The swell subsidence will not make possible any long-term comparison, but the short-term variations for the swell, associated with the long-term variations of the magma production rate, can provide pertinent information on the Hawaiian hot spot activity through time.

[4] The majority of studies concerning the Hawaiian hot spot have estimated these parameters for present day only. *Vogt* [1979] has calculated the present eruption rate at $0.1 \text{ km}^3 \text{ yr}^{-1}$ for Hawaii. *Davies* [1988] and *Sleep* [1990] have used an average estimation of the swell cross section and found a buoyancy flux for the Hawaiian hot spot of $B = 6.2 \text{ Mg s}^{-1}$ and $B = 8.7 \text{ Mg s}^{-1}$ respectively. Some attempts have been made to estimate both parameters all along the hot spot chain. *Bargar and Jackson* [1974] were among the first ones to calculate the volume of the volcanic edifices along the Hawaiian ridge. *Davies* [1992] has shown the variations of the buoyancy flux through time, by separating roughly the volcanic and swell contributions, on eight profiles along the Hawaiian chain. Many problems arise from these previous studies. One of the most important points is the uncertainty on the separation of the regional (swell) and residual (volcanic) contributions [*Smith*, 1990; *Wessel*, 1998], often leading to unreproducible results. Another problem is the fact that these studies did not take into account the volume of volcanic rocks included in the seamounts or islands compensating root. This leads to a strong underestimation of Q_v , and an overestimation of Q_s , by not subtracting this volume to the swell volume in the same region. *White* [1993] attempted a precise calculation of the melt production rate of the Hawaiian plume, assuming a local Airy compensation to estimate the total igneous volume. However, the initial edifices volumes were taken from *Bargar and Jackson* [1974], with the uncertainties explained above. An accurate estimation of the temporal variations of both the melt production rate Q_v and the swell volume flux Q_s thus remains undone.

[5] This paper proposes a precise determination of the temporal variations of the volume fluxes corresponding to 1) the magma production rate, including the volume of magma trapped in the compensating root, and 2) the rate of swell formation for the Hawaiian hot spot. After removing a subsidence model from the $2'$ bathymetric grid of *Smith and Sandwell* [1997], using seafloor ages from Müller's global age grid (version 1.3) [*Müller et al.*, 1997], we separate the swell contribution from the volcanic edifices with a new filtering method, based on a direct length scales separation. The volume of magma is then computed, taking into account the root volume by assuming either a local Airy compensation, or a regional flexural compensation (three-dimensional (3-D) elastic plate model). The volume associated with the swell is also determined. Both corresponding volume fluxes temporal evolution are calculated by translating windows along the chain. Finally, we discuss the correlation between these two parameters, and their respective use as a measure of the hot spot activity through time.

2. Topography of the Hawaii-Emperor Alignment

[6] The global topography (depth anomaly) corresponds to the bathymetry corrected from thermal subsidence, due to the

cooling of the oceanic seafloor when spreading away from mid-ocean ridges. We have used the $2'$ bathymetric grid of *Smith and Sandwell* [1997]. Over the Emperor-Hawaii chain, this grid contains mostly ship soundings data as illustrated by the dense ship track coverage in Figure 1 and our results will not be biased by the density and flexural models used to predict bathymetry from altimetry.

[7] Correction is deduced from subsidence models. As we need a global model for determining depth anomalies on the whole grid, we have chosen to consider the two most classical plate models: the PS model [*Parsons and Sclater*, 1977], giving the following theoretical depth d as a function of the age of the seafloor:

$$\begin{aligned} d(t) &= 2500 + 350\sqrt{t} & t < 70 \text{ Ma} \\ d(t) &= 6400 - 3200 \exp(-t/62.8) & t > 20 \text{ Ma}, \end{aligned} \quad (2)$$

and the GDH1 (Global Depth and Heat flow) model [*Stein and Stein*, 1992], which is defined with slightly different coefficients:

$$\begin{aligned} d(t) &= 2600 + 365\sqrt{t} & t < 20 \text{ Ma} \\ d(t) &= 5651 - 2473 \exp(-0.0278t) & t \geq 20 \text{ Ma}. \end{aligned} \quad (3)$$

These models only represent a rough tendency of the 'normal' seafloor, and display many drawbacks. The PS model includes points from the Bermuda and Hawaiian rise, too near hot spots to be unbiased [*Crough*, 1983], and fails to predict all the seafloor flattening at old ages. The GDH1 model does not take into account most of the bathymetric data for which the depth anomaly may be induced by a hot spot and uses a joint fitting of bathymetry and heat flow data, implying that the lithosphere is hotter and thinner than previously described. However, in its attempt to achieve a greater flattening at old ages, it predicts too much initial subsidence and a too early onset of flattening [*Smith and Sandwell*, 1997].

[8] No global subsidence model is able to take into account the flattening at old ages so it can explain all the bathymetric data. This is confirmed by the following observation: the seafloor does not flatten at the same rate everywhere, but rather has different behaviors, depending on its location, in particular from one subsidence corridor to another [*Marty and Cazenave*, 1989]. *Renkin and Sclater* [1988] have also pointed out this, using a very detailed and complete study of the depth and age relationship in the North Pacific. However, due to their limited database, they were not able to use an empirical relation derived from the data and finally decided to use the plate (PS) model. Their depths were corrected from sediment load but we can demonstrate that it does not change our results since the sediment cover over almost the entire Hawaiian ridge is thin and homogeneous.

[9] The choice of the reference surface taken for the ocean floor is critical as it can introduce an error in the next stages of our study. In order to estimate its influence, we have performed all calculations considering both *Stein and Stein* [1992] and *Parsons and Sclater* [1977] reference seafloor depth. Among the classical cooling models, they can be considered as end-members and thus are supposed to give a good estimate of residual depth variations. We have chosen by convenience to display only the resulting global

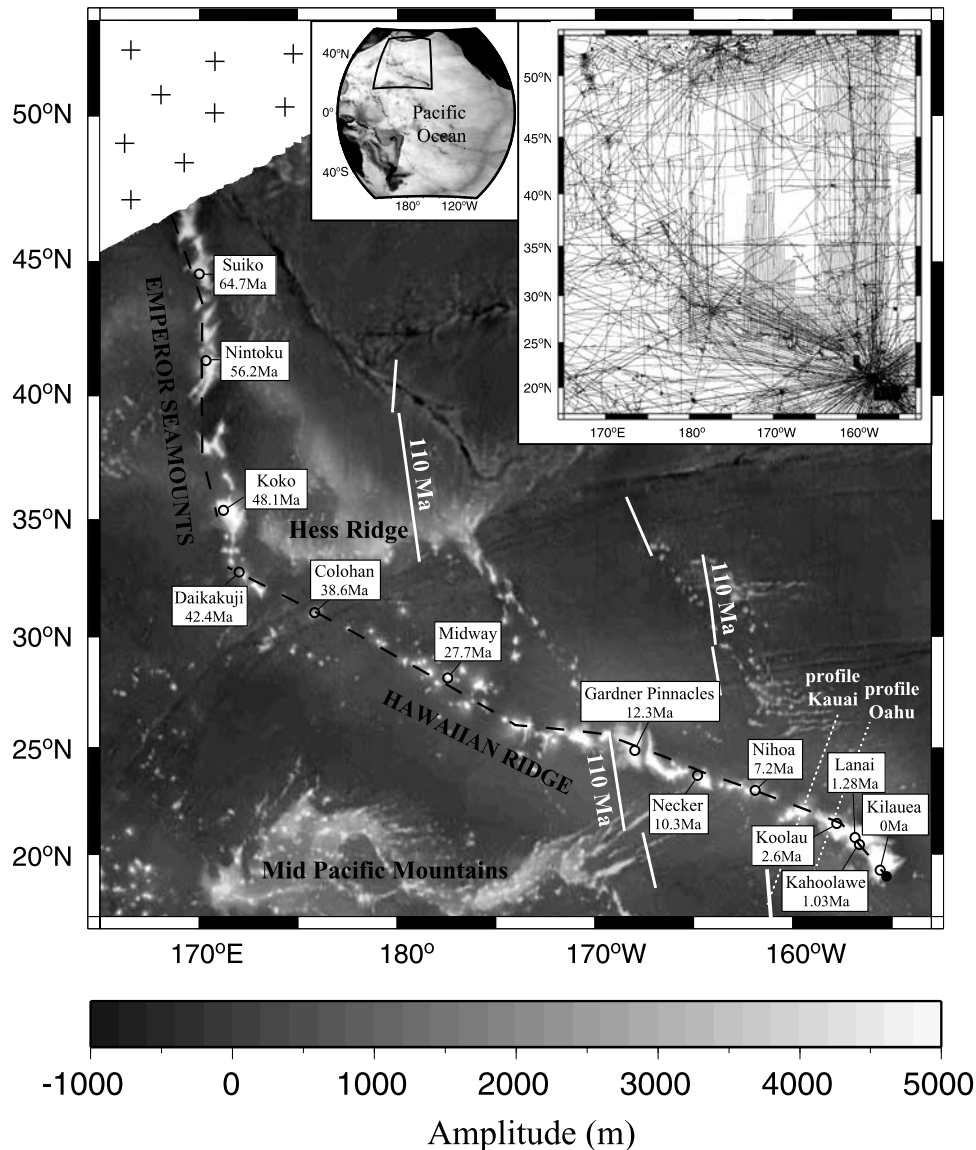


Figure 1. Global topography (depth anomaly) of the Hawaii-Emperor chain calculated with the GDH1 model (see text). The location is shown in the upper left inset, and the ship bathymetric coverage is displayed in the upper right inset. Short-wavelength (volcanism) and long-wavelength (swell) contributions to seafloor topography are clearly distinguishable. Ages of volcanism are given for the Hawaiian islands (Kahoolawe [Naughton *et al.*, 1980], Lanai [Bonhommet *et al.*, 1977], Koolau [McDougall, 1964; Doell and Dalrymple, 1973], Nihoa and Necker [Dalrymple *et al.*, 1974], Gardner Pinnacles [Garcia *et al.*, 1986], and Midway [Dalrymple *et al.*, 1977]) and for the Emperor seamounts (Colohan [Duncan and Clague, 1984], Daikakuji [Dalrymple and Clague, 1976], Koko [Clague and Dalrymple, 1973; Dalrymple and Clague, 1976], and Nintoku and Suiko [Dalrymple *et al.*, 1980]). The crosses represent regions with no seafloor age data. The dashed line is the trace of the Hawaiian hot spot along the chain. The black disk southeast of the chain represents the actual location of the hot spot.

topography obtained with GDH1 model (Figure 1). Next sections show that the choice of the subsidence model introduces differences in the swell amplitude determination, while it does not affect the calculated magma production rate.

3. New Determination of the Hawaiian Swell

[10] Large bathymetric features (swells) unrelated to standard cooling and subsidence, and wider than volcanic

features, are present in the topography obtained when correcting bathymetry from thermal subsidence (Figure 1). Figure 2 illustrates two possible configurations for a cross section perpendicular to the hot spot track: (a) the swell is formed like the seamounts by volcanic material, or (b) the swell is not generated by volcanism, and thus it has to be removed before further calculation.

[11] A shallow support mechanism has been originally suggested to explain the Hawaiian swell. The first mechanism invoked is a broad thickening of the oceanic crust by

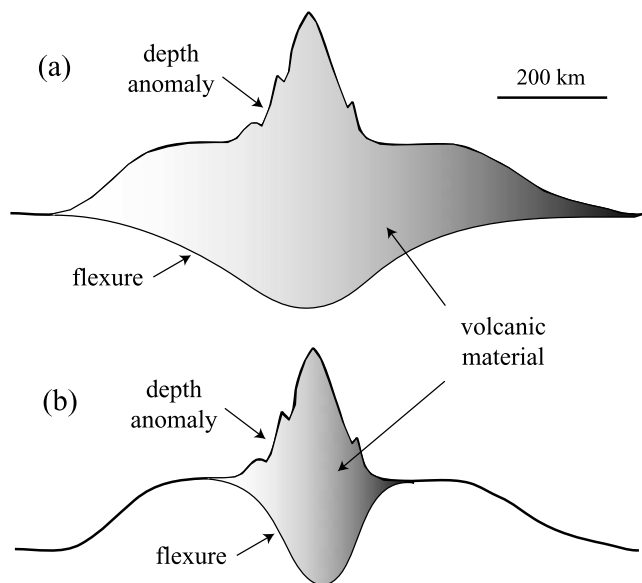


Figure 2. Sketch of a cross section perpendicular to the hot spot track showing two possible ways to calculate the volume of extruded material. (a) The swell must be taken into account in the volume computation. (b) The swell must be removed before any further calculation. The compensating root has been drawn here in the case of a flexural response of the lithosphere. The vertical scale is exaggerated.

lava flows emanating from the islands [Betz and Hess, 1942]. Later seismic refraction surveys indicated an uniform crustal thickness on the Hawaiian swell [Shor and Pollard, 1964]. Moreover, a seismic profile transversal to the Hawaiian hot spot track, across Oahu Island [Watts and ten Brink, 1989], demonstrates that Walcott's [1970] hypothesis of a flexural origin for the Hawaiian swell is not valid. Free-air gravity anomaly profiles from Watts [1976] confirm this result [Crough, 1983]. All studies lead to the same conclusion, that the swell is not created by volcanic material (Figure 2a), but has a deeper support mechanism [Morgan, 1971; Anderson et al., 1973]. Therefore it must be removed from the global topography before computing flexural or Airy compensating root, and calculating the magma production rate.

[12] A first cartography of depth anomalies in the North Pacific has been done by Menard [1973]. Afterward, many studies have been performed in order to have a precise determination of the amplitude of a hot spot swell. The different methods that attempt to isolate the swell component from the depth anomalies map can be divided into three different categories. First, and because the presence of a broad feature in topography implies a large length scale, low-pass convolutive filters have been used [Watts and Daly, 1981; Watts et al., 1985a; Cazenave and Dominh, 1987]. The most common among them is the Gaussian filter. However, these spectral filters remove only sinusoidal components of the data, so the residual (i.e., the seamount component removed by the filter) integrates to zero. No volume computation is therefore possible for the seamounts topography. Moreover, these filters are generally biased toward shallow values near seamounts. The second method is graphical: the parameters of a given shape (gaussian in

general) are determined in order to best fit a swell profile. Wessel [1993] approximated the profile of swell topography using super-Gaussians instead of the classical gaussian curves, which are known to overestimate the swell amplitude. However, this method can be applied on profiles only, usually taken transversal to the hot spot track, and needs strong assumptions on the shape of the swell topography. The third method consists of nonconvolutive filters, based on the fact that geophysical data of a given length scale usually contains many wavelengths, due to their topography far from a well-defined sinusoidal arch [Wessel, 1998]. These filters work on the spatial length scales of features, and not their spectral components, and provide a much better separation of the small length scales (seamounts) and large length scales (swell). Among them are the mean, median and mode filters. The mean filtering also tends to overestimate the broad features amplitude. The modal and median filters are recognized the most efficient to determine the topography of the swell amplitude. Sichoix et al. [1998] have used a modal depth analysis to find the seafloor swells and Superswell amplitudes in French Polynesia. However, in spite of some small bias toward the high topographic values, Smith [1990] demonstrates that the median filter is better than the modal one, for it is less noisy and more convenient to compute.

[13] The filtering method we introduce here, developed by C. Adam and V. Vidal (personal communication, 2002), belongs to the third category among the methods presented above. It corresponds to an improved use of the median 2-D filtering first described by Smith [1990]. Indeed, the main shortcoming of a median filter alone is its bias toward shallow depth values [Smith, 1990; Wessel, 1998], which can lead to a misinterpretation of the computed volumes of the swell and volcanic material, respectively, due to a wrong volume distribution. Therefore we have added a stage before the median depth anomaly filtering, in order to eliminate this unwanted bias.

[14] Seamounts elimination is performed through two different stages. During the first stage (minimization), the major part of the topographic features smaller than a given wavelength λ is eliminated by translating a $l \times l$ window along the whole topography grid. The translation step t is equal to the grid step. For each step, the value taken for the output grid at the present location is the minimum of the depth anomaly found in that window. The outer edges of the grid remain unchanged over a length $l/2$. A local minimum value in the depth anomaly grid therefore generates a $2l \times 2l$ area displaying this value in the minimized grid. If λ is the maximum topographic wavelength to eliminate, the condition on the size of the translating window is

$$2l \sim \lambda. \quad (4)$$

This stage tends to spread local minimum values of the depth anomaly. Therefore a compromise has to be found between i) a large l , removing efficiently the small-wavelength features, and ii) a small l , in order not to extend anomalous minimal values such as those introduced by fracture zones.

[15] A median filter from the Generic Mapping Tools (GMT) software [Wessel and Smith, 1991] is then applied

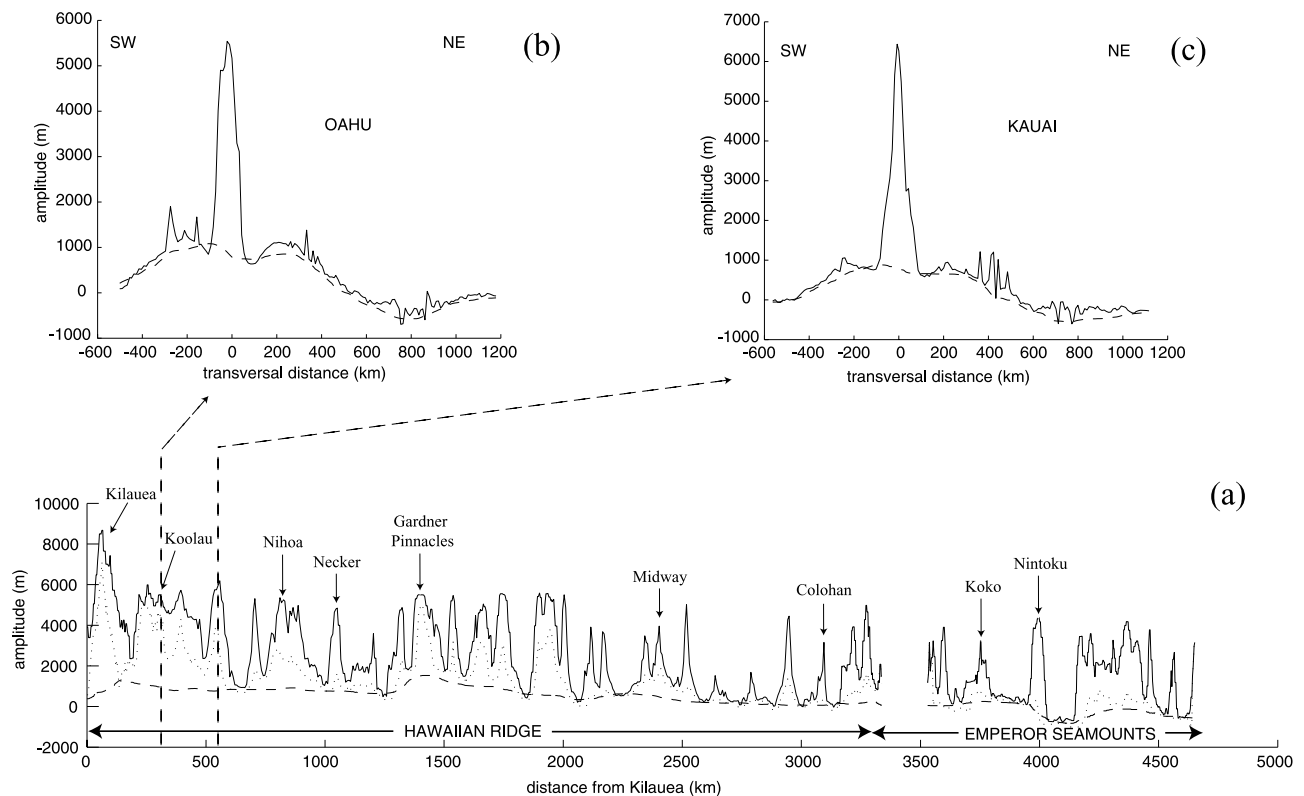


Figure 3. Depth anomaly obtained with the GDH1 subsidence model (solid line) and swell computed with our method (dashed line). (a) Profile along the hot spot track for the Hawaii and Emperor part of the chain (dashed line in Figure 1). The dotted line represents the amplitude along these profiles after the minimization stage (see text), and the dashed line is the swell amplitude found by our filtering method. (b) Transverse profile crossing Oahu Island (see Figure 1). (c) Transverse profile crossing Kauai Island (see Figure 1).

on the resulting minimized grid. It considers a disk of diameter $2R$ centered on each point, in which the median value is taken. This second stage smooths the shape and removes the remaining small-wavelength topography. In order to completely remove a wavelength λ , we must take [Wessel, 1998]

$$R \geq \sqrt{2}\lambda. \quad (5)$$

In order to test the robustness of the method, the influence of all parameters have been analyzed. No difference has been found when using different grid steps ($2'$, $4'$ and $8'$). l has been tested on a wide range: under 50 km, the depth anomaly is not sufficiently filtered, and for $l \geq 150$ km the influence of the fracture zones is too much amplified. In our computation, the translating window is 70×70 km wide, corresponding to the elimination of all topographic features smaller than about 140 km in extent. Similar tests have been performed for the parameter R of the median filter. A physically acceptable range of this parameter has been explored (not too large in order to keep the long-wavelength), and the best value is $R = 600$ km.

[16] Figure 3a shows the global topographic profile along the hot spot track, as well as the resulting minimized profile and swell profile. Two examples of transverse

profiles are shown in Figures 3b and 3c. The maximum amplitude on these profiles is about 1000 m. The amplitude of the swell in the Emperor region is found near or under zero: there is no swell on the older part of the Hawaiian-Emperor chain. The swell map for the whole region is presented in Figure 4, when correcting the initial bathymetric grid from the GDH1 model. The same map has been obtained with the PS model: even if the swell amplitude varies when using PS instead of GDH1, its spatial extension is not modified.

4. Local or Regional Compensating Root

[17] Seismic data, imaging the reflectors associated with the flexural profile [Watts *et al.*, 1985b; Lindwall, 1988; Watts and ten Brink, 1989] are not numerous enough to map the whole compensation surface under the Hawaiian Islands, and directly estimate the total volume of volcanic material. Hypotheses have thus to be made on the compensation mode, in order to compute the compensating root, and find the total igneous volume along the chain. Previous authors [Smith, 1990; White, 1993] have assumed a local Airy compensation, although White [1993] doubted of its validity for old lithosphere. We know that simple Airy compensation is not the actual compensation mechanism for the Hawaiian Islands [Watts and ten Brink, 1989], and a

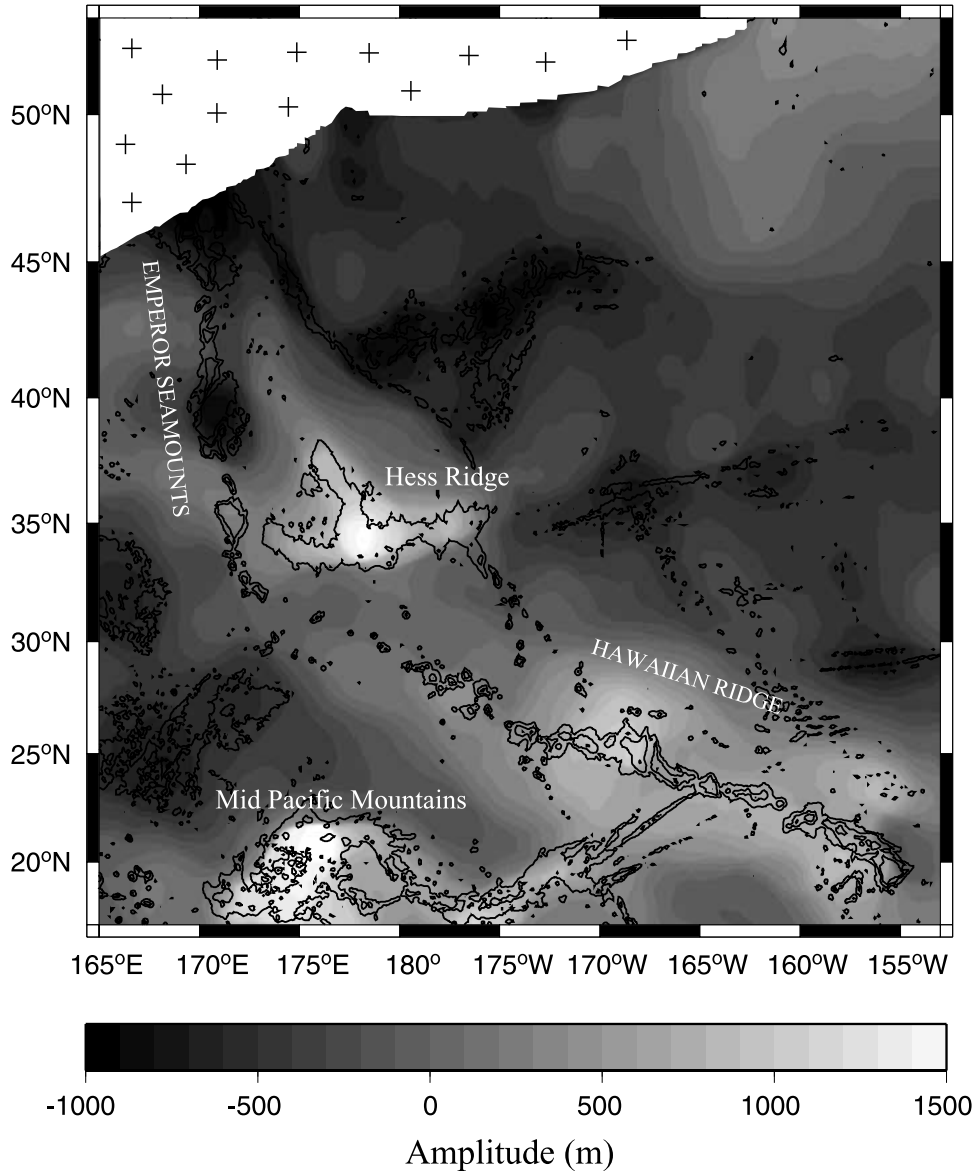


Figure 4. Map of the Hawaiian swell, obtained after removing the GDH1 subsidence model. Isobaths are drawn every 2000 m, from -6000 m to 4000 m. The crosses represent regions with no seafloor age data. The same map has been obtained using the PS model: The swell amplitude is modified but not its spatial extension (see text).

regional compensation by an elastic plate must be invoked [Watts *et al.*, 1980]. However, it can be proved that for volume computation, the Airy approximation gives the same result at all lithospheric ages.

[18] In order to confirm this nonintuitive assertion in the case of temporal variations computation, we have performed both calculations of volumes along the chain. Deformation w_{Airy} (positive downward) due to a local compensation is proportional to the topography h of the load itself:

$$w_{\text{Airy}} = \left(\frac{\rho_v - \rho_w}{\rho_m - \rho_v} \right) h, \quad (6)$$

where $\rho_v = 2800 \text{ kg m}^{-3}$, $\rho_w = 1030 \text{ kg m}^{-3}$ and $\rho_m = 3300 \text{ kg m}^{-3}$ are the volcanic load, sea water and mantle densities respectively. On the other hand, the three-

dimensional numerical approach developed by Watts *et al.* [1975] has been used to calculate the deformation w_{flex} caused by the loading of an elastic plate. Computation is performed in the Fourier domain, where this deformation can be written as a direct function of the size of the volcanic load H and the effective flexural rigidity D of the plate [Parker, 1973; McNutt, 1983]:

$$W_{\text{flex}} = (\rho_v - \rho_w) \left[\frac{(2\pi k)^4 D + (\rho_m - \rho_v)g}{g} \right]^{-1} H, \quad (7)$$

where $W_{\text{flex}}(k_x, k_y)$ is the deflection of the plate due to a topography $H(k_x, k_y)$, $g = 9.8 \text{ m s}^{-2}$ the acceleration of gravity and $k = \sqrt{k_x^2 + k_y^2}$ the wave number modulus. The flexural lithospheric rigidity D is linked to the elastic

thickness of the lithosphere T_e and depends mainly on the temperature, hence on the age of the lithosphere at the time of loading [Watts, 1978]:

$$D = \frac{ET_e^3}{12(1-\nu^2)}, \quad (8)$$

where $E = 8.10^{10}$ Pa is Young's modulus, and $\nu = 0.25$ is Poisson's ratio. Poisson's ratio is taken slightly different from the value $\nu = 0.5$ proposed by Lambeck and Nakiboglu [1981] for the incompressible model. Compressibility of the plate is thus included in our computation, which avoids an overestimation of the flexural parameter D for young volcanic loads [Nakada and Lambeck, 1986]. For an average lithosphere elastic thickness $T_e = 30$ km, the flexural rigidity is $D \sim 1.9 \times 10^{23}$ N m, a value commonly accepted for the Hawaiian Islands [Suyenaga, 1979; Turcotte and Schubert, 1982].

[19] To estimate the real flexure along the hot spot track is very difficult, because it should take into account the history of chain formation. Multiple episodes of volcanism in close proximity and even overlapping is sure to bias simple estimates of elastic plate thickness [Jordahl, 1999], and thus flexure calculation. Since we want a simple determination of the volume of volcanic material brought to the surface by the hot spot, we use a major simplification: we directly calculate the flexure created by the whole volcanic topography previously determined, and ignore the loading history. The elastic thickness corresponds to the isotherm 450°C [Watts, 1978], and therefore is given by

$$T_e = 3.1\sqrt{a_c}, \quad (9)$$

where a_c is the crustal age at the time of loading in Ma. Variations of T_e along the chain are taken into account. Deflection associated with the whole chain is then computed with the method presented below. Owing to our approximations, the resulting flexure does not correspond to the seismic reflectors and has no physical interpretation. However, the volume estimated is equal to the sum of the individual volumes calculated for each seamount.

[20] We demonstrate in the next sections that the volumes computed both with the local Airy compensation assumption or with the flexural root of a loaded 3-D elastic plate are closely the same. The morphology of the root is of course different, but the volume corresponding to the total igneous material remains unchanged, except for slight variations that will be discussed further in the paper. The main difference between the two results is that the flexure spreads the volumes associated with a volcanic load. We will focus on this aspect later on.

5. Temporal Variations of the Magma Production Rate

[21] In order to take into account the variations in lithospheric thickness at the time of loading along the hot spot track for the flexure computation, and to calculate the temporal variations of the volume of volcanic material in both local and regional compensation mode assumptions, we have used a method of translating windows along the hot spot trend. The trend here represents the main direction of

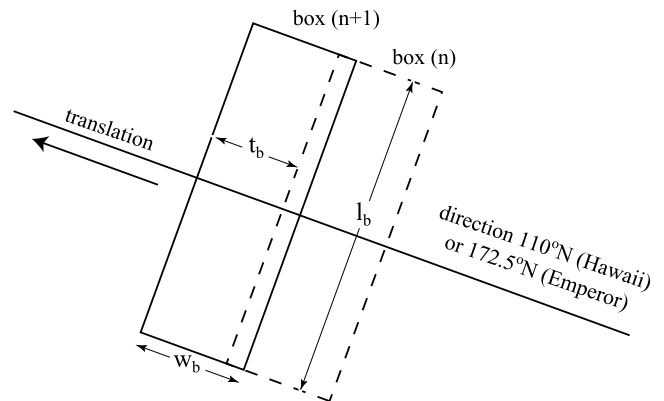


Figure 5. Temporal variation computation of T_e , Q_v , and Q_s along the chain: definition of the translating window parameters and orientation.

the hot spot on the Emperor and the Hawaiian part, taken respectively as 172.5°N and 110°N . The two main directions of the hot spot track have been used instead of the real hot spot track in order to simplify the computation. We consider windows of length l_b , width w_b and translation step t_b along the Emperor or Hawaiian trend (Figure 5). The length l_b is taken constant in all computations and large enough ($l_b = 10^\circ$) in order to include all the topographic features created by the hot spot and/or all the flexure spatial extension. Therefore considering a translation along the main hot spot direction (trend) instead of the hot spot track scarcely changes the volume calculation. Both topographies of the Hess Ridge and the Mid-Pacific Mountains, respectively north and south of the Hawaiian chain (Figure 1) are masked. Indeed, they do not belong to the surface expression of the Hawaiian hot spot, and keeping them into the swell and volcanic topography grids leads to an important overestimation of the volumes associated with both features, due to their vicinity. To avoid volume recovering, we have considered in all computations $t_b = w_b$.

[22] In order to quantify the influence of w_b , the Airy and flexural roots created by the volcanic load have been computed with $w_b = 1^\circ, 2^\circ, 4^\circ$ and 10° . For every computation, we translate the window along the Hawaiian and Emperor trends. For each window, in the flexural case, the deflection of the elastic plate due to the volcanic load present in this box is computed with $T_e(a_c)$, a_c being the age of the lithosphere at the time of loading, at the center of the window. The cumulated flexure, which represents the key parameter for the estimate of the volume of magma, is the sum of all the deflections. Very little flexural variations can be observed when changing the width of the windows w_b in the computation, which proves the robustness of the method. In the case of Airy compensation, the determination is much easier: the grid corresponding to the compensating root is merely obtained from the topography grid, by the way of equation (6).

[23] The volume flux of magma Q_v as a function of time is then computed in the following way. We translate again the window along the Hawaii and Emperor trends. The volume of magma for each box is the one included between the topography and the compensating surfaces, local (Airy) or regional (flexure). The corresponding period

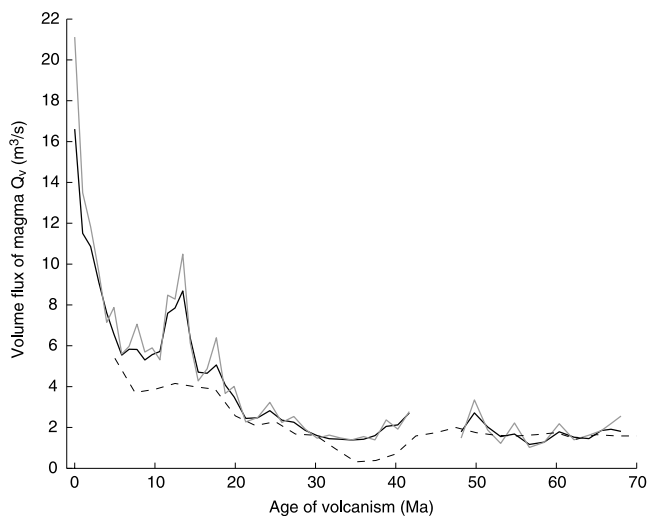


Figure 6. Temporal variation of the volume flux of magma calculated assuming a local (Airy) compensation (solid gray line) or a regional (flexural) compensation (solid black line). Short-term (~ 5 m.y. oscillations) and long-term (approximately exponential increase) behavior can be observed (see discussion). No volume flux is estimated near the bend (43–46 Ma) to avoid biased values due to the computation method at the Hawaii and Emperor trends crossing. The dashed line indicates the values found by *White* [1993], assuming an Airy compensation. Q_v values for ages younger than 3 Ma have to be considered carefully (see text for discussion).

of time ΔT during which it was produced is the difference in the ages of volcanism at the younger and older ends of the window. The black and gray lines in Figure 6 present the results for Q_v associated with the flexural and Airy compensations, respectively. The two curves show the same temporal evolutions for both calculations, except some differences in amplitudes. The curve associated with the local compensation (Airy) has a less smoothed behavior through time. This can easily be understood if considering the spatial distribution of the compensating roots in both case: for Airy compensation, the underlying root has the exact spatial distribution of the volcanic load, whereas for flexural compensation, the root associated with a single volcano is distributed over a wider space. This spatial distribution increases with the elastic thickness of the plate (i.e., with the age of the lithosphere at the time of loading): in the computation, the root volume corresponding to the volcanic load present in one translating window is spread over the neighboring windows, which leads to a smoother aspect of the final curve. Assuming an Airy compensation is therefore a better approach when estimating the melt production rate Q_v through time, for it localizes all the compensating root right under the associated overlying volcanic load. The volume computation in translating windows along the chain thus gives a more realistic idea of the temporal evolution of the igneous volume.

[24] In Figure 6, the melt production rate found by *White* [1993], who assumed a local Airy compensation, is also represented (dashed line). This estimation is systematically

below our result, in the Hawaiian part of the hot spot chain. Moreover, it seems to smooth the short-wavelength variations of periodicity ~ 5 m.y. One of the causes could be the use of the volumes of volcanoes determined by *Bargar and Jackson* [1974], who might tend to underestimate the surface volume of volcanic material. In our computation, when reducing the size of the window w_b , i.e., using more windows along the trend, the resolution of the curve logically improves, but the shape remains the same. Therefore for all the following study, we have considered the results with the smaller window width calculation only ($w_b = 1^\circ$).

[25] Two very different behaviors can be distinguished according to the Emperor or Hawaiian part of the chain. The production of magma is found mainly constant in the Emperor part, whereas it increases exponentially for the last 30 Ma. Moreover, in both regions some fluctuations can be observed, with a periodicity of about 5 m.y., except for a continuous increasing period slightly after the bend (from 38 to 23 Ma) and in the most recent volcanic activity (from 5 Ma until now). These features are discussed in the next sections. The increase by about an order of magnitude on the Hawaiian part was also found by *White* [1993] for the period 3–35 Ma, assuming a local compensation with a 2.5 Ma step along the seamount chain. Our values increase drastically for the last 5 Ma. However, our Q_v estimation for the most recent period (< 3 Ma) includes currently active volcanoes (Mauna Loa, Kilauea and Loihi) and should therefore be considered carefully. It is probable that in the youngest part of this region, isostasy is not valid anymore, due to the noninstantaneous response of the lithosphere to a surface load. A viscoelastic model where the rigidity decreases as the loading time increases should be used. The multilayered viscoelastic plate model of *Watts and Zhong* [2000] shows that this effect must be considered only for the first 100 k.y. after the onset of loading. In our case, this will induce a slight reduction of the total estimate of volume for the 3 Ma period and thus we choose to neglect it. We have also to mention that the swell amplitude could have been underestimated due to the presence of a deep trough northward of Big Island. This could have induced a slight overestimation of Q_v for this period.

[26] Neither a different hypothesis on the compensation mode, nor the variation of the relevant computational parameter w_b change the shape of the temporal evolution of the volume flux of volcanic material. Moreover, the result is independent of the choice of the thermal subsidence model (*Parsons and Sclater* [1977] or *Stein and Stein* [1992]), which underlines the efficiency of our filtering method (see section 3). However, it may not reflect directly the temporal evolution of the plume activity. Indeed, the volume of magma and its spatial distribution (island spacing) is controlled by surface parameters, in particular plate rigidity [*ten Brink*, 1991; *Hieronimus and Bercovici*, 1999].

6. Swell Evolution and Buoyancy Flux

[27] In order to check if the volcanic activity reflects the plume behavior, and therefore if our method is applicable as

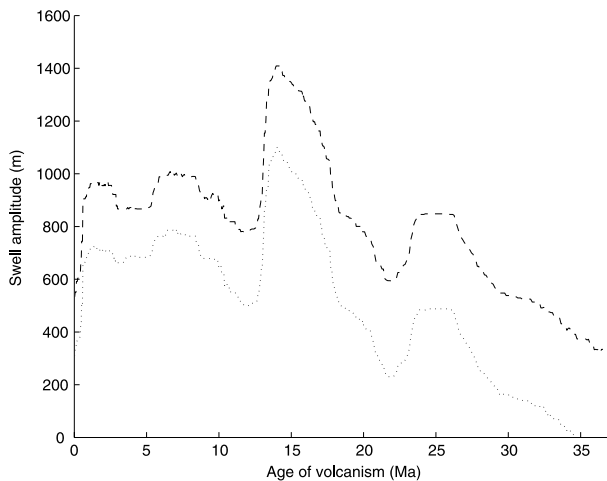


Figure 7. Temporal variation of the swell amplitude along the Hawaiian hot spot track for the PS (dashed line) and the GDH1 (dotted line) thermal subsidence models.

a characterization of the hot spot temporal evolution, we have computed the temporal evolution of the swell, which is supposed to characterize best the temporal evolution of the plume flux [Davies, 1992], using the same method. The direct analysis of the volume flux associated with the swell is difficult, not only because it depends strongly on the subsidence model used for the swell determination, but also because of thermal subsidence of the swell itself through time. This last phenomenon prevents the knowledge of the swell history all along the chain. Figure 7 gives the swell amplitude along the hot spot track from the swell grid calculated in section 3. The first observation is that despite the strong dependence on the subsidence model, the shape of the two swell amplitudes are the same: they follow a general decreasing trend from younger to older ages of volcanism. After 35–40 m.y., the swell has completely disappeared and the Emperor seamounts remain the only witnesses of the hot spot trace. Nonetheless, as previously noticed by Davies [1992], the swell does not monotonically subside with age as predicted by the model of Detrick and Crough [1978], but rather presents undulations that seem to be correlated with variations in volcanic activity. For instance, we observe the same peak around 13–15 Ma than in Figure 6, corresponding to the Gardner Pinnacles episode found by Vogt [1979] when estimating the eruption rate through the hot spot history. This peak can partially be explained by the change in plate motion that can be observed by the slight bend in Figure 1 between the longitudes 170°W and 175°W. However, no recent increasing is observed in the swell amplitude. Indeed, the swell is not yet totally formed under the most recent part of the chain, due to the nonnegligible onset time for thermal and/or dynamical swell support.

[28] The volume flux associated with the swell Q_s , corresponding to the volume between the reference floor and the swell, is computed with the same method (section 5). The temporal variations are given for the same translating window width $w_b = 1^\circ$. The results are presented in Figure 8. Almost no volume flux associated with the swell is observed for ages older than about 25–30 Ma (Figure 8). No swell is discernible along the Emperor seamount chain.

In this region, the buoyant material has been smeared out by horizontal shearing, which has been transverse to the Emperor chain since the change in plate direction 43 m.y. ago [Davies, 1992]. The general shape of the swell evolution in Figure 7 could be interpreted this way: the first 5 Ma correspond to the dynamic uplift centered on the plume (of radius ~ 500 km [Sleep, 1990]); and the following rough decreasing to both influences of gravitational spreading and conductive heat loss (for older ages).

[29] Equation (1) can be rewritten as a function of our parameters:

$$B = (\rho_m - \rho_w)Q_s, \quad (10)$$

where Q_s is the volume flux associated with the swell volume. The temporal evolution of the buoyancy flux calculated with equation (10), is shown in Figure 8. The buoyancy flux calculated by our method is smaller than the one proposed by Sleep [1990] or Davies [1988]. The major problem is that the determination depends strongly on the subsidence model. Moreover, the strength of our method, which works on 2-D grids instead of transverse profiles or rough estimations, becomes a weakness in the particular case of the swell volume calculation. Indeed, the swell volume is calculated as the volume of material included

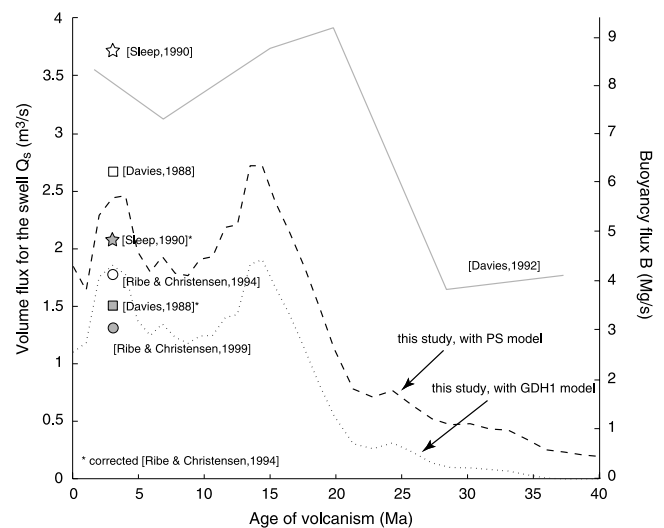


Figure 8. Temporal variation of the volume flux Q_s associated with the swell and of the buoyancy flux B when using the PS (dashed line) or GDH1 (dotted line) thermal subsidence model. The gray line is the rough curve found by Davies [1992] (six points along the chain for B). Open symbols show the determinations of B from Davies [1988] (squares), Sleep [1990] (stars), and Ribe and Christensen [1994] (circles). The solid square and star (*) are values from the same authors, corrected from the horizontal flux of buoyancy [Ribe and Christensen, 1994]. The solid circle is the same computation than the open one but taking into account the depletion buoyancy [Ribe and Christensen, 1999]. All symbols represent estimations of B for present day, without age precision given by the authors. We have chosen to represent them at 3 Ma, corresponding to the most recent swell maximum amplitude.

between the swell surface and the reference surface taken at $z = 0$. However, the swell grid contains regions of negative amplitude, due to deep flank moats, fracture zones, or merely problems linked to the choice of the subsidence model. Those regions are taken into account in the volume calculation, and tend to underestimate the total volume flux associated with the swell, and therefore the buoyancy flux itself. *Ribe and Christensen* [1994] best fitted the Hawaiian swell topography with their numerical model for $B = 4.1 \text{ Mg s}^{-1}$. Later, they took depletion buoyancy into account and estimated $B \sim 3 \text{ Mg s}^{-1}$ [*Ribe and Christensen*, 1999]. They suggested that current estimates of B were too high, due to the fact that they were based on the hypothesis that the vertical buoyancy flux B supplied by the plume is equal to the horizontal flux (due to plate motion) of buoyancy B_{swell} associated with the swell. The equivalence is relevant if the plume buoyancy is of thermal origin, but *Ribe and Christensen* [1994] showed that the horizontal flux of buoyancy B_{swell} associated with the swell topography can exceed by up to 80% the buoyancy flux B carried by the plume. This would give new values $B = 3.5 \text{ Mg s}^{-1}$ for *Davies* [1988] and $B = 4.8 \text{ Mg s}^{-1}$ for *Sleep* [1990] (also plotted in Figure 8). Our value is determined as a B_{swell} , and as so, remains underestimated. However, our global method of determination seems to act as a compensation between an underestimation due to the whole grid consideration, and an overestimation due to the hypothesis that the plume buoyancy flux is of thermal origin.

7. Estimation of the Plume Volume Flux

[30] Even with both estimations of the volume fluxes corresponding to the magma production rate Q_v and the rate of swell formation Q_s , it remains difficult to estimate the plume volume flux Q_p . The buoyancy flux determined by the swell volume estimation can far exceed the buoyancy flux carried by the plume [*Ribe and Christensen*, 1994]. Even if we admit a constant ratio between these two parameters, we still have the indetermination due to the choice of the thermal subsidence model. If the density anomaly in equation (1) is due to thermal expansion, the buoyancy flux can be rewritten as

$$B = \alpha \rho_m \Delta T Q_p, \quad (11)$$

where $\alpha \simeq 3 \times 10^{-5} \text{ }^\circ\text{C}^{-1}$ is the thermal expansion coefficient, ρ_m the mantle density, and ΔT the excess temperature. Both parameters Q_p and ΔT cannot be accessed independently.

[31] Geochemical considerations can provide information on the excess temperature. Hawaiian volcanoes provide evidence that the Hawaiian plume is zoned in terms of temperature and melting rate [*DePaolo et al.*, 2001]. The correlation between intershield differences in some incompatible element abundances ratios (La/Nb and Sr/Nb) and isotopic ratio, indicate that each shield has been formed from a compositionally distinct source [*Putirka*, 1999]. However, some of the intershield compositional differences reflect differences in mantle upwelling processes [*Frey et al.*, 1994], i.e., the systematic changes in the partial melting extent [*Eggins*, 1992]. Consequently, the excess temperature ΔT is not constant through the Hawaiian hot spot history

and we cannot deduce from equation (11) the temporal variations of the plume volume flux.

8. Discussion

[32] Temporal variations of the volume fluxes can be due to three different phenomena: 1) a change in the hot spot activity with time; 2) the sum of all superficial constraints (e.g., velocity of the plate, presence of fracture zones); 3) variations due to the oscillations that can appear when a hot plume interacts with an upper moving plate, leading for example to a periodical tilting of the plume. It is not easy to decorrelate these contributions in order to find the origin of the temporal variations.

8.1. Short-Term Variations

[33] Both temporal evolutions of the volume flux associated with the magma production Q_v and to the swell Q_s present undulations with a periodicity of about 5 m.y. A possible explanation could be the tilt of plume conduit through time, due to mantle advection generated by large-scale convection in the mantle [*Steinberger*, 2000]. According to *Whitehead* [1982], conduits should become unstable when tilted more than 60° from the vertical. These short-wavelength undulations in the volume flux could be generated by the oscillations of relaxation due to the periodic adjustment of the plume to plate motion [*Griffiths and Campbell*, 1991; *Skilbeck and Whitehead*, 1978; *Ihinger*, 1995]. However, even if the tilts can explain large variation in volume through time, their periodicity is still not well demonstrated. *Steinberger* [2000] shows that a plume may survive despite a tilt greater than 60° , depending on the surrounding mantle viscosity. An alternative explanation for these features is the ability of a plume conduit, deformed by large-scale motions in the mantle, to produce and propagate a variety of disturbances and instabilities, including solitary waves and diapir chains. These small structures, observed experimentally by *Olson* [1990], are often present in plume conduits [*Olson and Christensen*, 1986; *Schubert et al.*, 1989]. The rapid transport of geochemical heterogeneities by solitary waves [*Whitehead and Helfrich*, 1988] could explain the isotopic heterogeneity indicated by the $^{87}\text{Sr}/^{86}\text{Sr}$ - $^{206}\text{Pb}/^{204}\text{Pb}$ trend of Hawaiian shield lavas, which is not consistent with simple mixing of a plume and MORB-like components [*West et al.*, 1987]. A calculation by *Whitehead and Helfrich* [1990] estimates a pulse duration of approximately 7 m.y., comparable to our periodic variations.

8.2. Long-Term Variations

[34] The magma flow rate is approximately constant in the Emperor region (47–70 Ma). A recent geochemical study of lava composition along the Emperor Seamounts [*Regelous et al.*, 2003] suggests that the variations in the degree of melting from 85 to 42 Ma can be linked to the differences in lithospheric thickness. Therefore the plume activity can be considered constant over this period. No volume fluxes can be estimated in the region near the bend (43–46 Ma) because of the computation method, which would lead to overlapping windows, and thus a false estimation of the volumes. The striking increase of the volume flux of magma for ages <30 Ma (Figure 6) is not an effect of our computation: all variations of the parameters

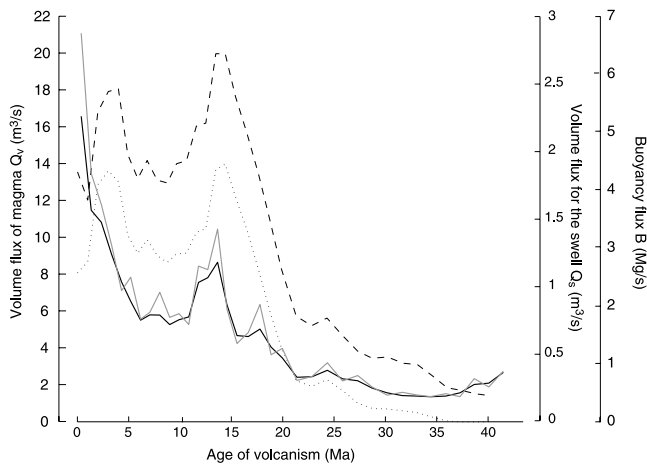


Figure 9. Correlation between the two calculated parameters: (1) temporal variation of the volume flux of magma (left axis) when assuming an Airy compensation (gray line) or a flexural deformation (black line) and (2) temporal variation of the volume flux Q_s , associated with the swell and buoyancy flux B (right axis) for the PS (dashed line) and the GDH1 (dotted line) thermal subsidence models. All values before 3 Ma are not reliable (see text).

linked to the swell determination, the translating window method or the choice of the subsidence model do not affect the shape of the evolution through time. The only slight overestimation occurs for the last 3 Ma, by considering the volumes associated with currently active volcanoes. As stated above, a viscoelastic model should be preferred for the last 100 k.y. [Watts and Zhong, 2000] and the swell determination might induce a bias toward a greater Q_v . The most recent Q_v values should therefore be taken with care. However, the general increasing trend from 30 Ma to present time remains. This confirms the result of White [1993], who has found the same shape when estimating the melt production rate through time assuming Airy isostasy, with the volumes estimated by Bargar and Jackson [1974].

8.3. Implications for the Hawaiian Hot Spot Activity

[35] After a period of almost constant production (70–47 Ma), the activity of the Hawaiian hot spot has strongly increased (last 30 Ma). Correlation in the temporal variations of volume fluxes associated with the magma production rate and to the swell (Figure 9) demonstrates that the excess temperature is not responsible for the important variations in both volume fluxes. Therefore it is the variation of the volume flux Q_p of material supplied by the plume itself that drives all other parameters.

[36] The swell and volcanic material volume fluxes reflect globally the same evolution. The calculation of the volume flux of volcanic material is thus a good indicator of the temporal variations in the hot spot activity. Moreover, it appears to be a more effective indicator than the volume flux associated with the swell, because it is independent of the choice of the subsidence model needed for its estimation.

9. Conclusion

[37] A precise determination of the temporal variations of the volume fluxes corresponding to the magma flow rate

and to the rate of swell formation for the Hawaiian hot spot has been performed. A new filtering method directly applicable to 2-D depth anomaly grids allows the separation of the swell and volcanic contributions. This leads to an estimation of the volume of magma produced by the Hawaiian hot spot independent of the subsidence model, and taking into account the volume of the compensating root. On older lithosphere, the compensating mode becomes more and more regional, and the shape of the underlying root is better approximated by a flexural approach. However, even in this case, the local Airy assumption remains the best way to estimate the magma production volume along the chain.

[38] Total volumes of volcanic material calculated for the Emperor and Hawaiian chains are $1.19 \times 10^6 \text{ km}^3$ and $5.89 \times 10^6 \text{ km}^3$ respectively. These values are about three times greater than the first estimations of Bargar and Jackson [1974] for 107 volcanoes along the Hawaiian Ridge-Emperor Seamount chain. This difference is essentially due to their method of estimation, which did not include the compensating root of the volcanoes.

[39] The study of temporal variations in magma production rate shows a striking increase from older ages until the last 3 Ma (a $\sim 300\%$ increase). The increase in melt production rate is even more drastic for ages < 3 Ma. Although real, this latter increase is probably slightly overestimated. The increasing shape is also present in the volume flux associated with the swell, but with a less marked increase at recent ages, due to the long time required for the complete swell formation. These results indicate a strong increase in the Hawaiian hot spot activity for the last 30 Ma. The 5 m.y. oscillations in the volume production can be explained either by plume tilting, or by the presence of solitary waves in the hot spot conduit. Geochemistry seems to be more in favor of the second hypothesis [Frey and Rhodes, 1993]. The intershield isotopic heterogeneities could therefore reflect intrinsic heterogeneities in the plume, brought to surface by the quick propagation of solitary waves.

[40] Correlation between both volume fluxes associated with the swell and with volcanic material demonstrates that the plume volume flux is responsible for temporal variations in magma flow rate. This latter parameter is easier to determine than the rate of swell formation, which has an intrinsic thermal evolution with age. The magma production rate thus appears as a relevant parameter in the characterization of the temporal variations of a hot spot activity.

[41] **Acknowledgments.** This paper has been greatly improved by the detailed comments of the AE David Sandwell and of the reviewers Walter Smith and Norman Sleep. A special thanks to W. Smith, who sent us the chapters of his Ph.D. thesis relevant to our paper. This paper also greatly benefited from several discussions with Anne Davaille, Neil Ribe, Cinzia Farnetani, and Vincent Courtillot. We are also grateful to Robert White and Jeroen van Hunen for their pertinent remarks. Finally, we wish to thank Claudia Adam for contributing to the elaboration and testing of the filtering method. This is IGP contribution 1957.

References

- Anderson, R., D. McKenzie, and J. Sclater (1973), Gravity, bathymetry, and convection in the Earth, *Earth Planet. Sci. Lett.*, *18*, 391–407.
- Bargar, K., and E. Jackson (1974), Calculated volumes of individual shield volcanoes along the Hawaiian-Emperor chain, *J. Res. U.S. Geol. Surv.*, *2*, 545–550.
- Betz, F., and H. Hess (1942), The floor of the North Pacific Ocean, *Geogr. Rev.*, *32*, 99–116.

- Bonhommet, N., M. Beeson, and G. Dalrymple (1977), A contribution to the geochronology and petrology of the island of Lanai, Hawaii, *Geol. Soc. Am. Bull.*, *88*, 1282–1286.
- Cazenave, A., and K. Dominh (1987), Global relationship between oceanic geoid and seafloor depth: New results, *Geophys. Res. Lett.*, *14*, 1–4.
- Clague, D., and G. Dalrymple (1973), Age of Koko Seamount, Emperor Seamount Chain, *Earth Planet. Sci. Lett.*, *17*, 411–415.
- Crough, S. (1983), Hotspot swells, *Annu. Rev. Earth Planet. Sci.*, *11*, 165–193.
- Dalrymple, G., and D. Clague (1976), Age of the Hawaiian-Emperor bend, *Earth Planet. Sci. Lett.*, *31*, 313–329.
- Dalrymple, G., M. Lanphere, and E. Jackson (1974), Contributions to the petrography and geochronology of volcanic rocks from the Leeward Hawaiian Islands, *Geol. Soc. Am. Bull.*, *85*, 727–738.
- Dalrymple, G., D. Clague, and M. Lanphere (1977), Revised age for Midway Volcano, Hawaiian volcanic chain, *Earth Planet. Sci. Lett.*, *37*, 107–116.
- Dalrymple, G., M. Lanphere, and D. Clague (1980), Conventional and $^{40}\text{Ar}/^{39}\text{Ar}$ K-Ar ages of volcanic rocks from Ojin (Site 430), Nintoku (Site 432) and Suiko (Site 433) seamounts and the chronology of volcanic propagation along the Hawaiian-Emperor chain, *Initial Rep. Deep Sea Drill. Proj.*, *55*, 659–676.
- Davies, G. F. (1988), Ocean bathymetry and mantle convection: I. Large-scale flow and hotspots, *J. Geophys. Res.*, *93*, 10,467–10,480.
- Davies, G. (1992), Temporal variation of the Hawaiian plume flux, *Earth Planet. Sci. Lett.*, *113*, 277–286.
- DePaolo, D. J., J. G. Bryce, A. Dodson, D. Shuster, and B. Kennedy (2001), Isotopic evolution of Mauna Loa and the chemical structure of the Hawaiian plume, *Geochem. Geophys. Geosyst.*, *2*(Article), 2000GC000133 [12,789 words].
- Detrick, R., and S. Crough (1978), Island subsidence, hot spots, and lithospheric thinning, *J. Geophys. Res.*, *83*, 1236–1244.
- Doell, R., and G. Dalrymple (1973), Potassium-argon ages and paleomagnetism of the Waianae and Koolau volcanic series, Oahu, Hawaii, *Geol. Soc. Am. Bull.*, *84*, 1217–1242.
- Duncan, R., and D. Clague (1984), The earliest volcanism on the Hawaiian Ridge, *Eos Trans. AGU*, *65*, 1076.
- Eggins, S. (1992), Petrogenesis of Hawaiian tholeiites. 2. Aspects of dynamic melt segregation, *Contrib. Mineral. Petrol.*, *110*, 398–410.
- Frey, F., and J. Rhodes (1993), Intershield geochemical differences among Hawaiian volcanoes: Implications for source compositions, melting process, and magma ascent paths, *Philos. Trans. R. Soc. London, Ser. A*, *342*, 121–136.
- Frey, F., M. Garcia, and M. Roden (1994), Geochemical characteristics of Koolau Volcano: Implications of intershield geochemical differences among Hawaiian volcanoes, *Geochim. Cosmochim. Acta*, *58*, 1441–1462.
- Garcia, M., A. Moser, P. Gurriet, and F. Frey (1986), Geochemistry of submarine glasses from the island of Hawaii: Inferences for source heterogeneity, *Eos Trans. AGU*, *67*, 1272.
- Griffiths, R., and I. Campbell (1991), On the dynamics of long-lived plume conduits in the convecting mantle, *Earth Planet. Sci. Lett.*, *103*, 214–227.
- Hieronimus, C., and D. Bercovici (1999), Discrete, alternating hotspot islands formed by the interaction of magma transport and lithospheric flexure, *Nature*, *397*, 604–607.
- Ihinger, P. (1995), Mantle flow beneath the Pacific plate: Evidence for seamount segments in the Hawaiian-Emperor chain, *Am. J. Sci.*, *295*, 1035–1057.
- Jordahl, K. (1999), Tectonic evolution and midplate volcanism in the South Pacific, Ph.D. thesis, 139 pp., Woods Hole Oceanogr. Inst., Mass. Inst. of Technol., Cambridge.
- Lambeck, K., and S. Nakiboglu (1981), Seamount loading and stress in the ocean lithosphere: 2. Viscoelastic and elastic-viscoelastic models, *J. Geophys. Res.*, *86*, 6961–6984.
- Lindwall, D. A. (1988), A two-dimensional seismic investigation of crustal structure under the Hawaiian Islands near Oahu and Kauai, *J. Geophys. Res.*, *93*, 12,107–12,122.
- Marty, J., and A. Cazenave (1989), Regional variations in subsidence rate of oceanic plates: A global analysis, *Earth Planet. Sci. Lett.*, *94*, 301–315.
- McDougall, I. (1964), Potassium-argon ages from lavas of the Hawaiian Islands, *Geol. Soc. Am. Bull.*, *75*, 107–128.
- McNutt, M. K. (1983), Influence of plate subduction on isostatic compensation in northern California, *Tectonics*, *2*, 399–415.
- McNutt, M. K. (1998), Superswells, *Rev. Geophys.*, *36*, 211–244.
- Menard, H. (1973), Depth anomalies and the bobbing motion of drifting islands, *J. Geophys. Res.*, *78*, 5128–5137.
- Morgan, W. (1971), Convection plumes in the lower mantle, *Nature*, *230*, 42–43.
- Müller, D., W. R. Roest, J.-Y. Royer, L. M. Gahagan, and J. G. Sclater (1997), Digital isochrons of the world's ocean floor, *J. Geophys. Res.*, *102*, 3211–3214.
- Nakada, M., and K. Lambeck (1986), Seamount loading of a compressible viscoelastic plate: An analytical solution, *J. Geodyn.*, *5*, 103–110.
- Naughton, J., G. McDonald, and V. Greenberg (1980), Some additional potassium-argon ages of Hawaiian rocks: The Maui volcanic complex of Molokai, Maui, Lanai and Kahoolawe, *J. Volcanol. Geotherm. Res.*, *7*, 339–355.
- Olson, P. (1990), Hot spots, swells and mantle plumes, in *Magma Transport and Storage*, edited by M. Ryan, pp. 33–51, John Wiley, Hoboken, N. J.
- Olson, P., and U. Christensen (1986), Solitary wave propagation in a fluid conduit within a viscous matrix, *J. Geophys. Res.*, *91*, 6367–6374.
- Parker, R. (1973), The rapid calculation of potential anomalies, *Geophys. J. R. Astron. Soc.*, *31*, 447–455.
- Parsons, B., and J. Sclater (1977), An analysis of the variation of ocean floor bathymetry and heat flow with age, *J. Geophys. Res.*, *82*, 803–827.
- Phipps Morgan, J., W. J. Morgan, and E. Price (1995), Hotspot melting generates both hotspot volcanism and a hotspot swell?, *J. Geophys. Res.*, *100*, 8045–8062.
- Putirka, K. (1999), Melting depths and mantle heterogeneity beneath Hawaii and the East Pacific Rise: Constraints from Na/Ti and rare Earth element ratios, *J. Geophys. Res.*, *104*, 2817–2829.
- Regelous, M., A. Hofmann, W. Abouchami, and S. Galer (2003), Geochemistry of lavas from the Emperor Seamounts, and the geochemical evolution of Hawaiian magmatism from 85 to 42 Ma, *J. Petrol.*, *44*, 113–140.
- Renkin, M., and J. Sclater (1988), Depth and age in the North Pacific, *J. Geophys. Res.*, *93*, 2919–2935.
- Ribe, N. M., and U. R. Christensen (1994), Three-dimensional modeling of plume-lithosphere interaction, *J. Geophys. Res.*, *99*, 669–682.
- Ribe, N., and U. Christensen (1999), The dynamical origin of Hawaiian volcanism, *Earth Planet. Sci. Lett.*, *171*, 517–531.
- Schubert, G., P. Olson, C. Anderson, and P. Goldman (1989), Solitary waves in mantle plumes, *J. Geophys. Res.*, *94*, 9523–9532.
- Shor, G., and D. Pollard (1964), Mohole site selection studies north of Maui, *J. Geophys. Res.*, *69*, 1627–1637.
- Sichoix, L., A. Bonneville, and M. K. McNutt (1998), The seafloor swells and Superswell in French Polynesia, *J. Geophys. Res.*, *103*, 27,123–27,133.
- Skilbeck, J., and J. Whitehead (1978), Formation of discrete islands in linear island chains, *Nature*, *272*, 499–501.
- Sleep, N. H. (1990), Hotspots and mantle plumes: Some phenomenology, *J. Geophys. Res.*, *95*, 6715–6736.
- Smith, W. (1990), Marine geophysical studies of seamounts in the Pacific Ocean basin, Ph.D. dissertation, Columbia Univ., New York.
- Smith, W., and D. Sandwell (1997), Global sea floor topography from satellite altimetry and ship depth soundings, *Science*, *277*, 1956–1962.
- Stein, C., and S. Stein (1992), A model for the global variation in oceanic depth and heat flow with lithospheric age, *Nature*, *359*, 123–129.
- Steinberger, B. (2000), Plumes in a convecting mantle: Models and observations for individual hotspots, *J. Geophys. Res.*, *105*, 11,127–11,152.
- Suyenaga, W. (1979), Isostasy and flexure of the lithosphere under the Hawaiian Islands, *J. Geophys. Res.*, *84*, 5599–5604.
- ten Brink, U. (1991), Volcano spacing and plate rigidity, *Geology*, *19*, 397–400.
- Turcotte, D., and G. Schubert (1982), *Geodynamics—Applications of Continuum Physics to Geological Problems*, 450 pp., John Wiley, Hoboken, N. J.
- Vogt, P. (1979), Global magmatic episodes: New evidence and implications for the steady-state mid-ocean ridge, *Geology*, *7*, 93–98.
- Walcott, R. (1970), Flexure of the lithosphere at Hawaii, *Tectonophysics*, *9*, 435–446.
- Watts, A. (1976), Gravity and bathymetry in the central Pacific Ocean, *J. Geophys. Res.*, *81*, 1533–1553.
- Watts, A. (1978), An analysis of isostasy in the world's oceans: 1. Hawaiian-Emperor seamount chain, *J. Geophys. Res.*, *83*, 5989–6004.
- Watts, A. B., and S. F. Daly (1981), Long-wavelength gravity and topography anomalies, *Annu. Rev. Earth Planet. Sci.*, *9*, 415–448.
- Watts, A. B., and U. S. ten Brink (1989), Crustal structure, flexure, and subsidence history of the Hawaiian islands, *J. Geophys. Res.*, *94*, 10,473–10,500.
- Watts, A., and S. Zhong (2000), Observations of flexure and the rheology of the oceanic lithosphere, *Geophys. J. Int.*, *142*, 855–875.
- Watts, A., J. Cochran, and G. Selzer (1975), Gravity anomalies and flexure of the lithosphere: A three-dimensional study of the Great Meteor Seamount, northeast Atlantic, *J. Geophys. Res.*, *80*, 1391–1399.
- Watts, A., J. Bodine, and N. Ribe (1980), Observations of flexure and the geological evolution of the Pacific Ocean basin, *Nature*, *283*, 532–537.

- Watts, A., U. ten Brink, P. Buhl, and T. Brocher (1985a), A multichannel seismic study of lithospheric flexure across the Hawaiian-Emperor seamount chain, *Nature*, *315*, 105–111.
- Watts, A., D. McKenzie, B. Parsons, and M. Roufousse (1985b), The relationship between gravity and bathymetry in the Pacific Ocean, *Geophys. J. R. Astron. Soc.*, *83*, 263–298.
- Wessel, P. (1993), Observational constraints on models of the Hawaiian hot spot swell, *J. Geophys. Res.*, *98*, 16,095–16,104.
- Wessel, P. (1998), An empirical method for optimal robust regional-residual separation of geophysical data, *J. Math. Geol.*, *30*, 391–408.
- Wessel, P., and W. H. F. Smith (1991), Free software helps map and display data, *Eos Trans. AGU*, *72441*, 445–446.
- West, H., D. Gerlach, W. Leeman, and M. Garcia (1987), Isotopic constraints on the origin of Hawaiian lavas from the Maui Volcanic Complex, Hawaii, *Nature*, *330*, 216–219.
- White, R. (1993), Melt production rates in mantle plumes, *Philos. Trans. R. Soc. London, Ser. A*, *342*, 137–153.
- Whitehead, J. (1982), Instabilities of fluid conduits in a flowing Earth—Are plates lubricated by the asthenosphere?, *Geophys. J. R. Astron. Soc.*, *70*, 415–433.
- Whitehead, J., and K. Helfrich (1988), Wave transport of deep mantle material, *Nature*, *338*, 59–61.
- Whitehead, J., and K. Helfrich (1990), Magma waves and diapiric dynamics, in *Magma Transport and Storage*, edited by M. Ryan, pp. 53–76, John Wiley, Hoboken, N. J.
- Wilson, J. (1963), A possible origin of the Hawaiian Islands, *Can. J. Phys.*, *41*, 863–870.

A. Bonneville and V. Vidal, Laboratoire de Géosciences Marines, Institut de Physique du Globe de Paris, Centre National de Recherche Scientifique, 4 place Jussieu, F-75252 Paris Cedex 05, France. (bonnevil@ipgp.jussieu.fr; vidal@ipgp.jussieu.fr)